Autonomous Aerial Water Sampling

John-Paul Ore and Sebastian Elbaum
Computer Science and Engineering, University of Nebraska, Lincoln, Nebraska 68588
e-mail: jore@cse.unl.edu, elbaum@cse.unl.edu
Amy Burgin
School of Natural Resources, University of Nebraska, Lincoln, Nebraska 68588
e-mail: aburgin2@unl.edu
Carrick Detweiler
Computer Science and Engineering, University of Nebraska, Lincoln, Nebraska 68588

Received 11 July 2014; accepted 1 March 2015

Obtaining spatially separated, high-frequency water samples from rivers and lakes is critical to enhance our understanding and effective management of freshwater resources. In this work, we present an aerial water sampler and assess the system through field experiments. The aerial water sampler has the potential to vastly increase the speed and range at which scientists obtain water samples while reducing cost and effort. The water sampling system includes 1) a mechanism to capture three 20 ml samples per mission, 2) sensors and algorithms for altitude approximation over water, and 3) software components that integrate and analyze sensor data, control the vehicle, drive the sampling mechanism, and manage risk. We validate the system in the lab, characterize key sensors, develop a framework for quantifying risk, and present results of outdoor experiments that characterize the performance of the system under windy conditions. In addition, we compare water samples from local lakes obtained by our system to samples obtained by traditional sampling techniques. We find that even winds of 5.8 m/s have little impact on the water sampling system and that the samples collected are consistent with traditional techniques for most properties. These experiments show that despite the challenges associated with flying precisely over water, it is possible to quickly obtain scientifically useful water samples with an unmanned aerial vehicle.

1. INTRODUCTION

Clean water is essential to our livelihoods, yet controlling water quality is an ongoing challenge. Water-borne diseases cause the death of 1.5 million under-5 children every year worldwide (The United Nations Children's Fund (UNICEF)/World Health Organization (WHO) & Wardlaw, 2009). The human-induced degradation of freshwater sources in the United States annually costs over $2.2 billion, but the full extent of the cost is poorly known due to insufficient data (Dodds et al., 2009). Part of the challenge is our lack of understanding of how water quality varies due to the spatial distribution of water transport pathways and contaminant source areas. Characterizing this large-scale variability remains a critical bottleneck that inhibits understanding of transport processes and the development of effective management plans to address water quality issues.

Our contribution to enrich our understanding of bodies of water is the development and assessment of an autonomous aerial water sampler, shown in Figure 1. This vehicle dramatically increases the ease, temporal resolution, and spatial scale of water sampling, a critical, pervasive, and expensive activity required to properly manage water resources.

The current state-of-the-art practice by limnologists and hydrochemists is to collect small water samples for lab analysis, since many of the properties they are interested in cannot be easily or cost effectively measured *in situ*. With these water samples in the lab, they can measure the chemical properties including phosphate, total phosphorus, nitrate/nitrite, nitrogen, and ammonia, as well as biological properties, such as the presence of toxic microcystins. Some properties can be measured in the field, but they require a literal boatload of equipment. These include temperature, conductivity, pH, dissolved oxygen, light, turbidity, and Secchi transparency. All of these field measurements, along with lab analysis, together present much of the canonical data through which surface water phenomena are understood (Eaton & Franson, 2005).

For example, our collaborators study the Fremont Sandpit lakes (see Figure 2). Each numbered lake is groundwater connected, surface water disconnected, chemically distinct, and must be sampled separately. Currently,

Direct correspondence to: Carrick Detweiler, carrick@cse.unl.edu

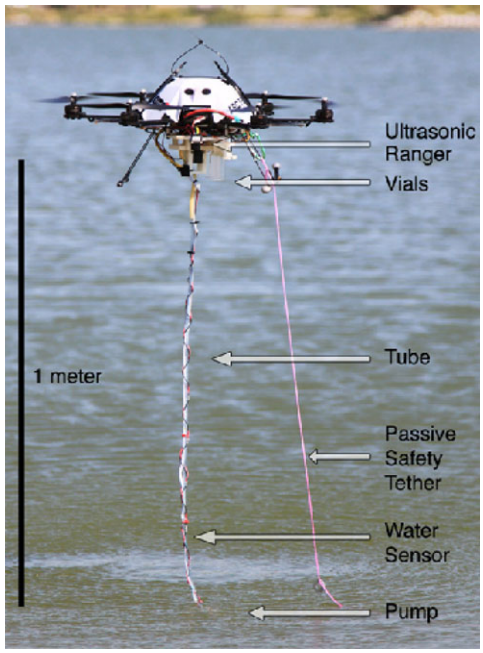

Figure 1. UAV-based water sampling.

Figure 2. Sandpit Lakes—Fremont, Nebraska.

a team of three scientists tow a boat to the lake, launch the boat, navigate to the sample location, collect samples and take measurements, dock the boat, get the truck, put the boat back on the trailer, and drive to the next lake. Each of 10–15 lakes is sampled in this manner over a long 10–15-hours day. But in just two hours, one scientist with our unmanned aerial vehicle (UAV) system could sample all these lakes, enabling the possibility of capturing data with unprecedented spatiotemporal resolution.

Current water sampling techniques are often based on grab sampling (e.g., dipping a bottle off the side of a kayak) (Wilde, Radtke, & (US), 1998), statically deployed collection systems (Erickson, Weiss, & Gulliver, 2013), or using mobile sensors affixed to autonomous surface vehicles (ASVs) (Dunbabin, Grinham, & Udy, 2009) or autonomous underwater vehicles (AUVs) (Bird, Sherman, & Ryany, 2007; Cruz & Matos, 2008). Most autonomous systems are used on large, open water features such as seas, large lakes, and rivers, and they sample for a long duration, in deep or distant places, with high quality. All of these methods are relatively slow, spatially restricted, costly, or difficult to deploy; no method samples quickly at multiple locations while overcoming barriers, such as dams or land.

Our approach is to come at the problem from the air. As shown in Figure 3, a scientist with a ground station computer specifies three GPS coordinates for water sampling and then the UAV flies to each location and samples water. As the vehicle navigates between sample locations, it can surmount obstacles such as dams, bridges, or land. To avoid cross contamination, the system pumps water and jettisons it overboard, flushing water from the current location through the pump and tube, as shown at steps five and seven. While flying, the system continuously monitors internal and external factors to determine the current risk level to avoid accidents. Once the mission is complete, the system returns to the ground station where the scientist can swap vials and start another mission.

In our approach, we use a micro-UAV that can be easily transported by the scientist in a car or backpack to the study site. These flying robots are computer-controlled, lightweight, commercially available, and can carry small payloads (< 750 g) for up to 20 min. Fortunately, a UAV's limited payload is not a critical shortcoming because water samples do not have to be very large ($20\,\text{ml} = 20\,\text{g}$) to be scientifically useful, as shown by the wide range of applications identified in Table I. Also, the UAV's battery-limited flights allow it to travel nearly a kilometer and back, which is close enough for many water-sampling applications.

Obtaining water samples from a UAV, however, poses challenges that must be addressed before these systems can be deployed in the wild. In our previous work, we delineated those challenges and presented the overall concept of UAV-based water sampling (Ore, Elbaum, Burgin, Zhao, & Detweiler, 2013). This article extends that work by providing a more detailed and precise account of the system, performing more extensive studies (over three times the number of flights) including an analysis of the impact of wind, developing a logical framework for quantifying risk, and updating and extending most results based on the experiments performed over the past year. More specifically, the contributions of this work include the following: 1) developing a UAV-based system that autonomously obtains three 20 ml water samples per flight, 2) integrating and characterizing sensors on the UAV to enable reliable, low-altitude flight (1.0 m) over water, 3) developing a framework to quantify risk, 4) testing the system both indoors in a motion-capture room as well as in over 90 flights in the field at lakes and waterways, 5) characterizing the system outdoors in wind, and 6) validating that key water chemical properties are not biased by using a UAV-based mechanism. We also discuss

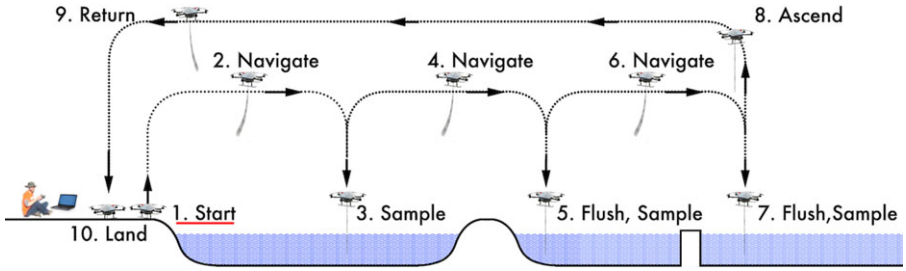

Figure 3. Overview of the proposed method.

Table I. Water sampling applications summary.

Task	Sample Size	Frequency	Spatial Domain
Limnology	15 ml–1 L(Eaton & Franson, 2005)	variable	local, regional, and global
Environmental Monitoring	15 ml–5 L (Wilde et al., 1998)	variable	surface and ground water
Oil Spills	30–50 ml (ITOPF, 2012)	month-years	surface water
Disease Tracking	10–100 ml (WHO, 2004)	once	open wells, rainwater systems
eDNA	15 ml–10 L (Pilliod, Goldberg, Laramie, & Waits, 2012)	once, few	Lagoons, rivers, streams, lakes

lessons learned and identify a number of outstanding challenges to be addressed in future work, such as determining the impact of waves and flowing water on altitude control.

2. RELATED WORK

Our work is part of a larger class of aerial manipulation tasks, all of which interact with the environment by touch. Such applications have become an area of intense study, including efforts to grasp while flying (Jimenez-Cano, Martin, Heredia, Ollero, & Cano, 2013; Thomas, Polin, Sreenath, & Kumar, 2013), carry collectively (Michael, Fink, & Kumar, 2011; Ritz & D'Andrea, 2013), and turn valves (Orsag, Korpela, Bogdan, & Oh, 2014). Unlike these efforts, we do not account for the dynamics of our interaction with the environment, since the dangling tube in water exerts negligible force. Instead our focus is on system robustness, safety, and ensuring the scientific validity of the readings. Other efforts relate to this work in one of two ways: either an autonomous vehicle is used to take samples in aquatic environments, or a UAV is controlled at low altitude. We treat first the former and then the latter.

Autonomous vehicles used in water sampling are typically either autonomous surface vehicles (ASVs) or autonomous underwater vehicles (AUVs), both deployed in water features such as oceans or large lakes. For example, The Lake Wivenhoe ASV (Dunbabin et al., 2009; Dunbabin & Grinham, 2010) is capable of navigating throughout complex inland waterways and measuring a range of water quality properties and greenhouse gas emissions. Underwater, the MARES AUV (Cruz & Matos, 2008; Melo & Matos, 2012) dives up to 100 m deep to monitor pollution, collect data, capture video, or follow the seabed. Other efforts such as the NIMS system (Rahimi et al., 2004) explore semimobile sensor networks providing adaptive sampling. Another approach is to combine sensor networks with autonomous vehicles (Zhang & Sukhatme, 2007). These vehicles and systems are good for long-duration sampling in deep or distant places. However, it is time-consuming and expensive to frequently redeploy these systems. In contrast, our system can be carried in a backpack and quickly deployed to sample multiple disconnected water features from a single launch site. Further, *in situ* sampling cannot yet measure all desired water properties (Erickson et al., 2013), such as the presence of suspended solids, pathogens, and heavy metals.

Other UAV control systems related to our effort (Merz & Kendoul, 2013) fly at low altitude in rural areas. Their system, like ours, utilizes extended state machines (Harel, 1987; Merz, Rudol, & Wzorek, 2006) and likewise contains events indicating an unsafe circumstance, and transitions to a state seeking safe recovery.

Our system does not incorporate obstacle avoidance, as we neither build nor update a map. However, this is an area of intense study, both outdoors (Ross et al., 2013; Scherer, Singh, Chamberlain, & Saripalli, 2007; Scherer et al., 2012; Schmid, Lutz, Tomić, Mair, & Hirschmüller, 2014) and indoors (Bachrach, He, & Roy, 2009; Bills, Chen, & Saxena, 2011; Shen, Michael, & Kumar, 2011). Further, recent advances in occupancy grids such as OctoMaps (Wurm, Hornung, Bennewitz, Stachniss, & Burgard, 2010) provide a more efficient representation of obstacles at various scales. Most of these systems devote significant payload to sensors

and processing, but as components become smaller and lighter, we intend to utilize advances from these efforts in future versions of our system.

Other recent efforts for UAV height estimate include miniature radar altimeters, optical flow, and laser altitude estimation (Kendoul, 2012). The lightest commercially available radar altimeters are still 160 g, (350 g with enclosure—heavy for a micro UAV) and are accurate to only ± 0.5 m, below the requirements of our system. Using an off-axis rotating laser flying low over a river (Jain et al., 2013) yields ≈ 1 cm altitude accuracy by looking for specular returns to estimate the plane of the water. This method simultaneously builds an occupancy grid for obstacle avoidance. However, sensors consume much of the payload. Traditional laser altimeters, which direct a single beam toward the ground, are easily perturbed by poor reflections and ambient light over water, so instead we chose ultrasonic rangers.

Our system flies with a small dangling pump. The flight dynamics of cable-suspended loads with UAVs can be stable (Faust, Palunko, Cruz, Fierro, & Tapia, 2013; Sreenath, Michael, & Kumar, 2013), but our system avoids this by hanging a sufficiently small mass (10 g), which incurs small forces relative to those generated by our UAV.

Some multirotor UAVs take off from and land in calm water (Aquacopters, 2012; QuadH2O, 2014). We do not adopt these platforms or attempt to harden our system to be waterproof because 1) fast-moving water or waves might make it impossible to take off, 2) the sampling mechanism and battery enclosure would be complete sealed, making removal difficult and decreasing the efficiency of swapping vials or batteries, and 3) radio strength attenuates near the water's surface, and we want the UAV and base station in constant contact so that users can monitor the system and comply with UAV regulations.

Another low-altitude UAV akin to ours (Göktoğan et al., 2010) surveils and sprays aquatic weeds at low altitude using a RUAV ("rotary UAV," i.e., a scale helicopter) with a laser altimeter. Our work similarly does not address global planning and requires a human expert to decide where to perform tasks (weed experts in Göktoğan's case and lake experts in ours). Our work differs from this in that we use ultrasonic with pressure for altitude, since laser altimeters work poorly at short range over clear water, and we retrieve a liquid rather than depositing it. In addition, we focus on validating the system's utility for water scientists.

Our earlier publication on aerial water sampling (Ore et al., 2013) is the first description of using UAVs for water sampling, to our knowledge. Subsequent to our effort, another group (Schwarzbach, Laiacker, Mulero-Pázmány, & Kondak, 2014) explored aerial water sampling using UAVs. Using a small-scale helicopter (1.8 m rotor), they arrive at an overall similar design, with a dangling pump and a water payload as close to the center of gravity as possible. Their work explores the control architecture and does not directly address measuring altitude over water, field testing, or wind resilience. Their larger vehicle can carry 500 ml of water but is less portable and deployable by field scientists.

Flying over water is inherently risky. Several efforts in the automated systems and robotics domain have developed strategies to manage and mitigate risk. At the highest level, we note the system engineering frameworks developed by institutions such as NASA (Dezfuli et al., 2011; Dorofee, Walker, Alberts, Higuera, & Murphy, 1996), which focus on "identify-analyze-plan-track-control" loops to relate and decompose *individual risks* as they affect *performance risks*. More specifically to the robotics domain, we note efforts tailored for particular contexts. For example, risk management has been implemented for robot arms as a "risk field" (Lacevic & Rocco, 2010) or "danger criterion" (Kulić & Croft, 2005) as they get close to a person, or more commonly as a "risk function" (Montemerlo, Pineau, Roy, Thrun, & Verma, 2002; Sattar & Dudek, 2014) that is meant to minimize risk by estimating the cost of acting on poorly understood human input and, when a certain threshold is exceeded, requiring the human to reiterate the input. We build on these concepts of risk factor decomposition and identification, risk assessment, and mitigation actions. More specifically for unmanned aerial systems (UASs), tabulations of failures and their frequencies (Clothier & Walker, 2012) seek to characterize incidents and their severity. This is still difficult as few failures are disclosed and documented, and because UASs encompass a myriad of emerging systems. Like this approach, we tabulate our experience in the field in the form of positive tests to identify previously seen operational space, and we use our experience to help us identify potential risk factors. Unlike this approach, we do not assume that our system will behave like other UASs in general, due to the particularities of our system in a rare application domain with limited prior data.

3. TECHNICAL APPROACH

Through discussions with our hydrologist partners, we derived a set of four key high-level requirements for the aerial water sampler: 1) carried and operated by a single scientist, 2) autonomously capture at least three 20 ml water samples at predefined locations within a 1 km range, 3) does not bias water properties when compared with current practices, and 4) cost-effective enough to prompt the shift of current practices.

Through this work we start addressing these requirements. The prototype we have developed can be operated by a single scientist, collect the required samples without biasing water properties, and increase the temporal and spatial scale of collection to make it more cost-effective than current practices. Still, as we shall describe in future work, this aerial water sampler does not completely cover all the requirements as, for example, it still lacks the front end to facilitate its operation by scientists, it is not resilient to all types of weather, and it cannot gather deep-water samples.

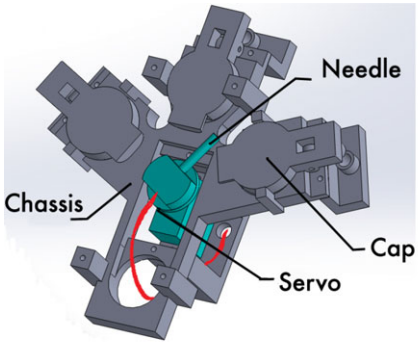

(a) Sampling mechanism.

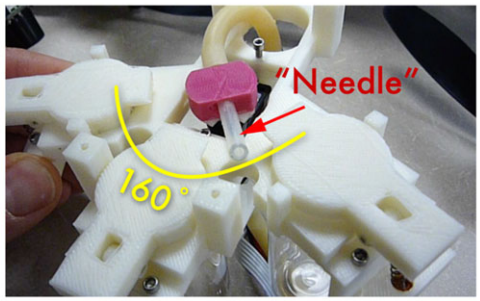

(b) Rigid plastic tube to direct water flow: the 'Needle'.

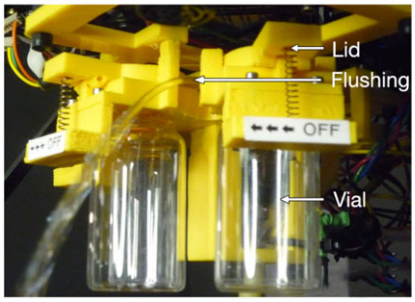

(c) 'Flushing' water to clean system.

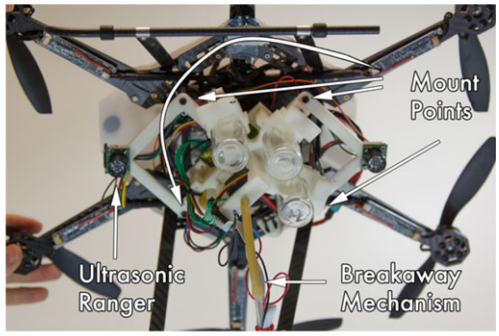

(d) Subsystem details including mounting points.

Figure 4. Mechanical design: key elements.

Our current system requires constant contact with a ground station to accelerate rapid prototyping, but processing could be moved onboard at the expense of mission duration since we have 150 g of available payload. We find a ground station acceptable at this stage of development since flying beyond line-of-sight is currently prohibited by U.S. aviation authorities.

While keeping these limitations in mind, we now describe how we address these requirements through the following: 1) mechanical design of the sampling mechanism in Section 3.1, 2) sensor configuration and characterization for near-water flight in Section 3.2, 3) altitude estimation over water in Section 3.3, 4) framework for risk management in Section 3.4, and 5) software systems, including logic used to ensure that the vehicle stays out of the water in Section 3.5.

3.1. Design of UAV Water Sampling Mechanism

The water sampler is built onto an AscTec Firefly (Achtelik, Doth, Gurdan, & Stumpf, 2012), a hexrotor with a maximum payload of 600 g. Total flight time is 15–20 min. The Firefly comes equipped with GPS, three-axis accelerometers and gyroscopes, a compass, and an air pressure altimeter. This UAV communicates with a human backup pilot using a radio link, and it has two 2.4 GHz 802.15.4 radios for remote autonomous control and sensor feedback.

The water sampling mechanism is held together by a "chassis" shown in a three-dimensional (3D) rendering in Figure 4(a). The chassis holds three 20 ml screw-top glass vials, spring-hinged lids, a servo to direct the water, and it has mount points for the dangling tube, embedded controller, and ultrasonic range sensors. The "chassis" is made of 3D printed ABS plastic and integrates with the airframe at four mount points, as shown in Figure 4(d).

Water flow is directed to the vials through a servo-controlled plastic tube called the "needle." Figure 4(b) shows how the servo confines the rotation of the needle in a plane and can rotate 160° total, 80° from center in either direction. We constructed the vial chambers so that the servo-rotated needle lifts the lid, and once the needle rotates away from the vial, a spring holds the lid closed. As shown in Figure 4(b), the servo rotates the needle into one of five predefined positions: three vial-filling positions and two water-jettisoning positions, which flush water through the system, cleaning it between samples. Flushing is shown in Figure 4(c). We have two gaps for flushing: between vials one and two, and between vials two and three. By having two gaps, we reduce the risk of cross-contamination by never moving the needle past a lid that seals a filled vial. The duration of the flushing phase is configurable,

defaulting to 20 s, three times the duration required to fill a 20 ml vial.[1]

The needle is connected to a 1.05 m plastic tube hanging below the UAV with a micro submersible water pump (TC-SMicropumps, 2014) attached at the end of the tube. We chose the length of the 1.05 m tube as this was a good balance between the length of the tube and the flow rate (7.5 ml/s at 1.05 m) when supplied with voltage ranges recommended by the manufacturer. We selected a flexible tube that could bend enough to curl under the UAV during landing, while remaining rigid enough to dampen motion-induced oscillations. The tube is mounted below the center of mass of the unloaded vehicle to minimize changes in flight dynamics while pumping.

A breakaway mechanism, shown in Figure 4(d), allows the pump and tube mechanism to release if subjected to greater than 15.1 N of force. This is somewhat less than the maximum UAV lifting thrust of $\approx$ 17.7 N. This prevents the UAV from getting stuck if the pump becomes entangled in the environment. So far, all entanglements have worked themselves free before the breakaway released.

To protect the pump from becoming clogged by small rocks or aquatic plants, we enclose it in a sewn mesh filter to form a bag around the pump. This is especially useful when pumping in shallow water, where the pump frequently hits the bottom. We tried different grains of mesh, and we found that finer grained meshes ($< 500\ \mu$ m) inhibit flow by capturing air bubbles when submerged. Larger-grained meshes ($\geq$ 2 mm) allow particles or pebbles that can block and perhaps damage the pump. We chose a 1-mm-grained mesh to protect the pump while allowing flow.

3.2. Sensors for Near-water Flight

Flying near water is dangerous to the UAV because it can damage the electrical and mechanical systems, yet flying near water is absolutely necessary to sample water. It is difficult because the UAV does not come equipped with sensors to detect its surroundings, especially anything below it. More specifically, to fly close to water, we need a more accurate altitude estimate than the UAV's built-in pressure altimeter. The built-in pressure altimeter readings drift multiple meters over the time of a flight and are therefore insufficiently accurate to fly near water. We considered various altitude sensors (as discussed in Sec. 2), and we chose ultrasonic rangers and water conductivity sensors to improve our height estimation. We use two Maxbotix MB1240-EZ4 ultrasonic rangers (Maxbotix, 2014) pointing straight down and flanking the sampling mechanism 10 cm from the center to increase the likelihood of an unobstructed path to the water's surface, which might otherwise be blocked by the swinging tube and pump. The ultrasonic pulse propagates in the shape of a cone, and this particular model has the smallest cone available of approximately 60°. The shape of the cone is important because we want the sensor to detect only what is immediately below it, and not the tube, which is below it at a small angle.

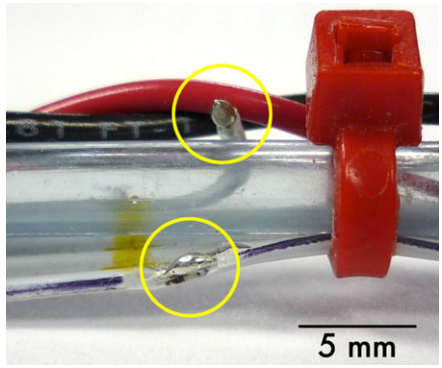

Figure 5. Water conductivity sensors.

A problem with narrow cone ultrasonic sensors is that they stop sensing reliably when not pointing straight down. At large pitch or role angles, $> 20^\circ$ at an altitude of 1.0 m, the ultrasonic wave reflects away from the vehicle and the sensor reports MAX_RANGE. We address this large angle problem by rejecting large measurements. In practice, such extreme angles are rare while hovering, and we plan missions to approach the water from above rather than flying close to the water at a steep attack angle.

Each ultrasonic ranger samples at 10 Hz, and we offset their sample time by 50 ms to prevent interference. This also increases the rate that altitude information is acquired to 20 Hz. This rangefinder is well suited to rotorcraft because of its resilience to motor noise, $\pm$1 cm accuracy, and reliability within 2 m.

In addition to keeping the vehicle dry, another reason why it is important to have accurate altitude is that the pump must be submerged and primed prior to operation. To know that the system is actually touching water and not just approaching dry ground, and as an additional safety system, we augmented the system with water conductivity sensors, as shown in Figure 5. We place water conductivity sensors every 10 cm from the bottom of the sample tube, up to 50 cm, to ensure that the system knows when it is too close to the water. The conductivity sensors also govern the pump. An onboard controller turns on the pump only after being wet for more than 400 ms, which allows it, as experimentally determined, to prime.

By using ultrasonic sensors and conductivity sensors together, we have an accurate, affordable, redundant sensor configuration for near-water altitude estimation. The full characterization of these sensors over water is provided in the next section.

[1]Initial experiments show that 20 s flushing avoids cross-contamination. We plan to rigorously characterize this in future work.

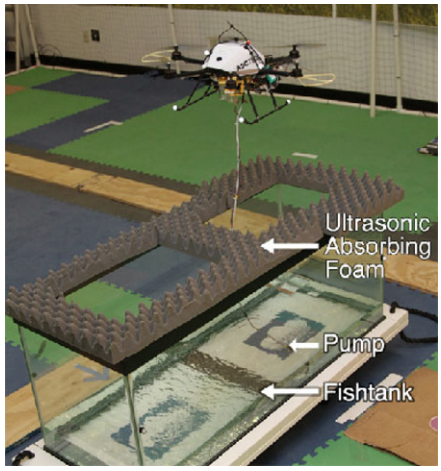

Figure 6. Indoor testbed for water sampling.

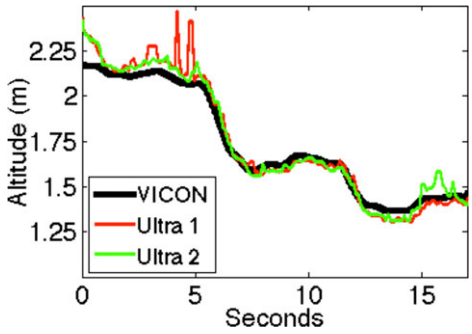

Figure 7. Altitude over a fish tank.

3.3. Altitude Estimation Over Water

Even after we add sensors to sense below the UAV, the sensors might read incorrectly because we have added a tube that can swing in front of the sensor during flight, and a pump that can generate other dynamics. We could encounter wind gusts, low battery, weak radio signals, sensor noise, or the pump could become entangled with the environment. These problems might appear individually or in any combination. We knew from the beginning that if we adopted a method such that we do not land in the water intentionally, then altitude estimation to sample water would be critical so that we do not land in the water unintentionally. This is why the physical design emphasizes redundant range sensors with additional conductivity sensors so that multiple measurements confirm our altitude estimate and increase the likelihood of a successful sampling result.

To form an altitude estimation over water, we started by characterizing the ultrasonic sensors during flight over water without the dangling tube and pump. To simulate being over a river or lake, we purchased a fish tank and filled it with 10 cm of water. Our indoor testbed is shown in Figure 6 inside our Vicon motion capture room. We placed acoustic foam over the edge of the fish tank to absorb the ultrasound waves and ensure the tank is not detected. Then we created a program to fly the UAV over the fish tank so we could compare the ultrasonic to Vicon altitudes. The results are shown in Figure 7, during which the UAV was over water, and the ultrasonic readings are shown offset by 15 cm, the height of the water in the fish tank. The data were gathered during autonomous flight, flying the UAV to 2 m above the fish tank, then descending to 1.5 m and then 1.25 m.

As seen in Figure 7, the ultrasonics closely follow Vicon ground truth, although they lag $\approx$ 180 ms behind as the UAV descends. The lag is caused by the latency of the ultrasonics, but the lag is less important for our system since we are most concerned with accurate readings when the UAV is hovering, and we limit the descent velocity so that the system has more time to detect the water's surface. In some cases, as shown near 5 s, the ultrasonics exhibit spikes. This is relatively rare, sometimes caused by the dangling tube, and typically occurs at longer ranges (+1.85 m), and becomes more pronounced above 2.5 m. We have found that it rarely effects both sensors simultaneously, but having more than one sensor is important to filter sporadic noisy readings.

Based on these findings, we form an altitude estimate in two ways. First, at low altitude we utilize a Kalman filter of ultrasonic ranger and pressure sensor readings. Second, at high altitudes, we use the pressure sensor plus an offset from the low-altitude Kalman estimate. Figure 8 shows an overview of the altitude formation process.

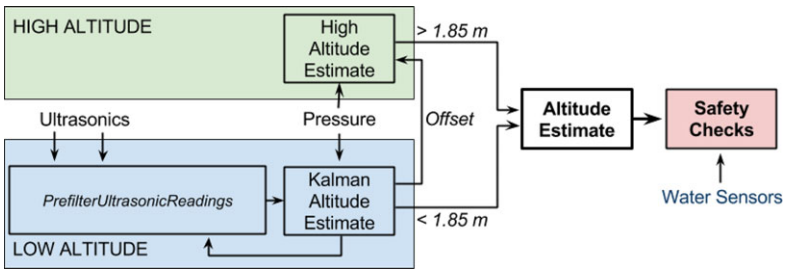

Figure 8. Altitude estimation information flow.

Algorithm 1 Prefilter sensor readings to avoid non-Gaussian noise and spurious readings. Although our current system uses only two ultrasonics, this procedure supports multiple sensors.

```
1:  procedure Prefilter Ultrasonic Readings (ultrasonicReadings, currentKalmanEstimate)
2:      maxRange = 1.85                                                    ▷ meters
3:      proximityThreshold = 0.075                                         ▷ meters, empirical
4:      varianceThreshold = 0.08                                           ▷ meters^2, empirical
5:      numUltra ← 2
6:      bestScore ← −1
7:      sumOfBestReadings ← 0
8:      countOfBestReadings ← 0
9:      for i ← 1, i ≤ numUltra, i ← i + 1 do                              ▷ iterate over all ultrasonics
10:         ultrasonicScore[i] ← 0                                         ▷ Initialize
11:         if ultrasonicReadings[i] < maxRange then                       ▷ ensure range
12:             ultrasonicScore[i] ← 4                                     ▷ highest priority
13:         end if
14:         if abs(currentKalmanEstimate − ultrasonicReadings[i]) < proximityThreshold then   ▷ proximity
15:             ultrasonicScore[i] ← ultrasonicScore[i] + 2                ▷ medium priority
16:         end if
17:         if abs(getVariance(ultrasonicReadings[i], 1 sec) < varianceThreshold then   ▷ variance
18:             ultrasonicScore[i] ← ultrasonicScore[i] + 1                ▷ least priority
19:         end if
20:         if ultrasonicScore[i] > bestScore then
21:             bestScore ← ultrasonicScore[i]                             ▷ track best score so far
22:         end if
23:     end for
24:     for i ← 1, i ≤ numUltra, i ← i + 1 do                              ▷ iterate to find all best scores
25:         if ultrasonicScore[i] = bestScore then
26:             sumOfBestReadings ← sumOfBestReadings + ultrasonicReading[i]
27:             countOfBestReadings ← countOfBestReadings + 1
28:         end if
29:     end for
30:     bestValue ← sumOfBestReadings/countOfBestReadings                  ▷ average
        return min(bestValue, maxRange)                                    ▷ input to Kalman Filter
31: end procedure
```

We employ a scoring heuristic to prefilter the ultrasonic readings, because of non-Gaussian noise and incorrect readings when the flexible tube swings in front of an ultrasonic sensor or at higher altitudes. We observe three types of errors: first, as mentioned above, we observed spikes above 1.85 m; second, when flying, especially in wind when the vehicle has higher pitch or roll, one of the ultrasonics can be continuously blocked by the tube, causing readings far away from our prior estimates; third, periodic views of the tube cause a burst of low readings and high variance. Rather than model the non-Gaussian noise, we assume that at any time only one of the two sensors will be occluded by the dangling pump. We also assume the two sensors yield nearly identical values when not occluded, because of their physical placement.

To choose between the sensor readings, we use a scoring heuristic. Our heuristic is shown as pseudocode in Algorithm 1. Starting on line 11, we give strongest preference to values within the maximum range (< 1.85 m), then on line 15 we score based on proximity to the current estimate (within 0.075 m), then on line 18 we give weak preference based on tolerable variance during the last one second (< 0.08 m^2). If more than one sensor has the same score, we average the readings.

The datasheets for the Maxbotix MB1240-EZ4 ultrasonic rangers indicate a maximum range of 8 m, but in practice when mounted near UAV propellers we empirically determined a maximum range of 1.85 m. We determined the proximity threshold by examining the maximum observed difference between continuous readings of the two sensors when flying over typical terrain and especially when changing altitude. For the variance, we performed flights with aggressive maneuvers and observed the variance induced during partial occlusions of the ground by the swinging tube. These thresholds together help select the sensor reading that satisfies the linear and Gaussian-noise assumptions of a basic Kalman filter.

The final altitude estimate uses the Kalman estimate at low altitude and the pressure sensor with an offset at high altitude, as shown in Figure 8. At low altitudes, the Kalman estimate is accurate enough to assure vehicle safety, while at high altitude, the pressure sensor is sufficient, and if sensor drift sends the system below 2 m, the low-altitude controller will take over. Anytime the vehicle transitions from low to high altitude, the pressure sensor is offset with the last best estimate from the Kalman filter. When descending, we limit velocity so that the UAV can stop before coming within 1 m of the water.

We enforce additional safety checks with the water sensors on the tube. If the water sensors indicate that the tube is too deep, then the UAV ascends to a safer altitude. The water sensor data are not directly added to the Kalman filter both because they are slow (0.5 s) and also because occasional water droplets from the pump cause false readings. In Section 4 we validate this approach with indoor and field experiments.

3.4. Risk Management

We approach risk and risk management as a technical challenge of the same order as mechanical design, sensors characterization, and software architecture. Our approach is to adopt a level of risk management that matches the scale of our endeavor and leverages our experience building and operating the system. Our aerial water sampler is meant to operate over water, and it can resist some light water splashes, but it was not designed to be water-resistant. As a result, falling into the water is one of the system's largest risks, one that we have designed against by incorporating a variety of sensors (described in Section 3.2) to supply data about the distance to the water, and by adopting a conservative approach to fuse and use that information. Still, we are concerned that factors such as the wind, the distance to the safety operator, the presence of obstacles in the vicinity of the operating area, the water load on the system, sensor variability, and other elements that we could not anticipate or cost-effectively design for could significantly affect the system operating risk.

To assess and mitigate risk, we build on the notion of Sattar & Dudek (2014) regarding *assessors*, i.e., functions that can map variables' values to quantified risks. We extend that approach taking into consideration that 1) the likelihood that particular inputs resulting in Loss of Vehicle or Loss of Mission are as yet poorly understood, 2) positive test cases can help delineate the boundaries of known and less risky operational space, 3) we want the system to take precautionary actions without necessarily requiring human intervention, and 4) we want to account for specific foreseen risks and general unforeseen risks within one logical framework.

Given a system S, let V denote the set of variables that can be known or measured by S. These variables and their values constitute the basis on which a system developer can assess risk through the use of *assessor* functions. Using an assessor κ, the system developer can determine the quantity of *individual risk*, ρ, a non-negative real number, contributed by certain variables values as determined by κ. That is, $\kappa : V' \subseteq V \rightarrow \rho$. An assessor κ could be as simple as a function that identifies the maximum value for a variable or could be more complex, such as a polynomial over the derivative of multiple variables. The weighted sum of all individual risks, the *total risk*, is denoted by τ. The total risk is then $\tau = \sum_{i=1}^{|K|} cont_i \rho_i$, where $cont_i$ determines how much each individual risk contributes to τ. The system developer can then use the individual risks ρ or the total risk τ to determine how and when to respond with actions to mitigate risk. More specifically, given a list of available mitigating actions $A = (\alpha_1, \alpha_2, \ldots, \alpha_j)$, the developer defines risk response functions that map risk to specific action sequences to be triggered when thresholds for ρ or τ are reached. The functions take the form of $f : (\rho, \tau) \rightarrow \overline{B}$, where $\overline{B} = [\alpha : \alpha \in A]$.

Table II. Examples of water-sampling variables.

Variable Description	Data Type
Altitude (z)	float
Velocity in z	float
Conductivity Sensors (Water Sensors)	int (5)
Ultrasonic readings	{float, float}
position x, y	{float, float}
Battery level	float
Is overwater	boolean
Wind speed mean 2-s	float
Wind speed mean 5-s	float
Prevailing wind speed (2-min mean)	float
Prevailing wind direction	float
Gust factor	float
Satellite count	int
Absolute distance UAV-User	float
Manhattan distance UAV-Base	float
x, y distance to obstacle	float
Radio strength - radio n	float[int]
Mass of UAV system including water (g)	int

In the context of our aerial water sampling system, Table II captures the set of variables we considered. Our assessors operate on some of these variables, and come in two forms: expert and learned. Expert assessors address risky circumstances we expect to encounter, such as the distance from the UAV to the water, which we assume is riskier with increasing proximity. Learned assessors stem from our previous work (Jiang et al., 2013), wherein we use positive test cases to learn invariants in system variables, and automatically generate monitors. These boundaries are then automatically detected and encoded into an assessor.

Table III. Examples of water-sampling actions.

Type	Action
Specific	Reset target sampling altitude
Specific, General	Limit velocity down
Specific, General	Increase altitude
Specific, General	Slow xy
Specific, General	Return to base
Specific	Extra flushing
Specific	Reboot embedded system
Specific	Move upwind from obstacle

Furthermore, learned assessors can be formulated to describe more intricate relationships such as derivatives, temporal properties, or the shape of publisher-subscriber graphs. As a matter of illustration, here are four of the key assessors we implemented that provided individual risks:

$$Expert : \kappa_{Water-proximity}(Altitude(z), ConductivitySensors, WindSpeed) \rightarrow [0, 1],$$

$$Expert : \kappa_{Observability}(DistanceUAV - User, Altitude(z), WindSpeed) \rightarrow [0, 1],$$

$$Learned : \kappa_{UAV-velocity}(UAV - pitchVelocity, UAV - rollVelocity, UAV - zVelocity) \rightarrow \{0, 1\},$$

$$Learned : \kappa_{State-transitions}(FiniteStateMachineOfSystem OperatingStates) \rightarrow \{0, 1\}.$$

The first two assessors were defined by us, while the last two were automatically inferred based on the traces collected during system testing. The risk values returned by the expert assessors are real numbers between 0 and 1, and binary values for the learned assessors (they generate a value of 1 when an invariant is violated). Surprisingly, and as it will be shown in the experimental section, the wind did not turn out to be as significant a factor in system operation and success rate as we suspected. Distance to the safety operator, on the other hand, was an obvious risk-increasing factor, as judging the distance from the system to the water when observing from longer distances became more challenging, making the operator jittery or too slow to react. We explore this further in Section 4.3. Table III contains some of the actions we mapped to risk values, where each action is classified as being targeted by individual or general risks. For example, if $\kappa_{Observability} < minAcceptableObservability$, then $ReSetTargetSamplingAltitude = BaseAltitude + (1 - \kappa_{Observability}) * coefficient$, that is, if observability is below a threshold, then the target sampling altitude is increased in proportion to the decreased visibility.

3.5. Software Architecture

The high-level software architecture is shown in Figure 9(a). The software system can be thought of as having two parts: 1) code on a ground station using the robot operating system (ROS) that handles low-level communication with the UAV, mission control, risk management, navigation, state machines, and altitude estimate; 2) code on an embedded controller attached to the UAV that receives instructions from the ground station, controls the water-sampling subsystem, reads ultrasonic and water sensor data, and broadcasts the water-sampling subsystem state. These two parts communicate with one another via XBee radio links. Both subsystems incorporate assessors to detect high-risk water sampling or navigating conditions based on the sensor readings, and they restart a mission. In total, the system includes about 7K lines of C, C++, and Python code.

At a high level, the software system implements a finite state automata (FSA) as shown in Figure 9(b). These states together are an abstraction of the behavior of the whole system. Each oval in the figure represents a logical state, which is encoded in the software as a configuration of ground control and embedded system software. The arrows in the figure represent state transitions, labeled with high-level descriptions of the event that triggers a transition from one state to another. The flow of activities is clockwise starting from the OFF state in the upper-left corner.

From OFF, the system starts when the UAV and ground station are ready, and then the control flows to MISSION CONTROL. If a mission is available, the system transitions to the NAVIGATING state, where the UAV takes off and goes to a GPS location. Once the UAV arrives at the sample location (waypointAchieved), the system moves to the DESCENDING state. When the target height has been reached, the system tries to detect water (WAIT FOR H2O - FLUSH), and once water is detected, water is flushed through the tube to clean it. After flushing completes, the systems starts PUMPING, where it captures water in a vial and starts or stops the pump based on whether the conductivity sensors report H2O or noH2O. After pumping, or if the system takes too long to pump, or if the altitude ever goes too low (highRisk), then the system transitions to the ASCENDING state. This moves the vehicle up away from the waters surface and the possible danger of getting wet. After ascending, the system returns to MISSION CONTROL and either starts a new mission or returns to base and ends the program.

The software coordinates these activities through: 1) waypoints, which are compared to the measured location of the UAV, so that the UAV arrives at the desired sample location and descends to the target height; 2) timers, which track how long the pump has actually been pumping and

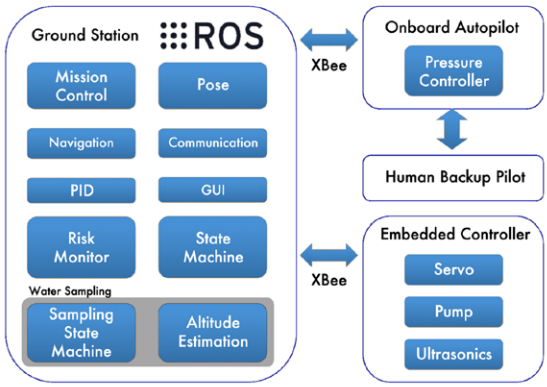

(a) High-level organization of software architecture.

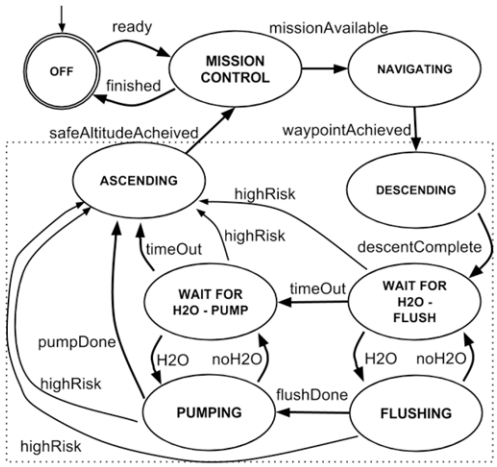

(b) Whole system finite state automata with sampling states. Dotted Box surrounds the water-sampling portion of the state machine.

Figure 9. Software and state machine overview.

infer that the tube has been sufficiently flushed or that the vial is full; and 3) assessors on sensor values to measure risk and ensure the sampling altitude is safe.

4. EMPIRICAL ASSESSMENT

In this section, we assess four different aspects of the aerial water sampler. We start by evaluating the system capabilities to stay at the target altitude while sampling in Section 4.1. In Section 4.2 we start to assess the system effectiveness in collecting samples. Next, we analyze the system performance while manipulating the target sampling altitude under various wind speeds ranging from 0 to over 5 m/s in Section 4.3. Last, we compare the water sample properties when collected by hand versus with the aerial water sampler in Section 4.4.

4.1. Maintaining Altitude While Sampling

The outdoor altitude control assessment was conducted on a human-made waterway along Antelope Creek in Lincoln, NE. The water at this location is 1–2 m deep. For these outdoor tests we chose a calm day with wind speeds measured at less than 0.27 m/s with a hand-held anemometer.

We recorded the ultrasonic, pressure sensor, and Kalman-filtered height estimate, as shown in Figure 10. During this study, the UAV always flew at low altitude. This figure shows the UAV while it "approaches" the sample destination and the critical "sample" stage when the UAV descends and maintains altitude to pump water. Compared with altitude tests indoors, the ultrasonic sensor readings had more spikes, indicating additional noise,[2] but the dual ultrasonics still allowed for successful altitude control. The figure also shows the depth of the pump, as detected by the water sensors on the tube. Both the first and second water sensor are activated during sampling, but never the ones above. We noticed that the water sensor skimmed the surface as the UAV approached the sample location, which is reflected in Figure 10. During the outdoor altitude tests, we observed a larger variation in x and y during sampling due to GPS inaccuracy, which impacts height as the UAV tilts as it tries to adjust its location. These tests confirm that our filtered altitude estimate works well at near proximity to water in calm conditions.

4.2. Water Sampler Effectiveness

We tested the water sampling system effectiveness both indoors and outdoors. Indoors, we perform autonomous missions that launch the UAV to 2.0 m, fly over the fish tank (Figure 6), descend to the sampling height where the pump is submerged, take a sample, and then ascend back to 2.0 m. Each test consisted of three samples, and afterward the water sample vials were checked. Any amount less than the top of the "neck" of the sample vial was recorded as less than full. We completed a total of 30 trials. Each trial took 4–5 min flying, with an additional 5–10 min to set up the system, empty the vials, and periodically change batteries.

Table IV summarizes the results. Overall, from the 90 consecutive collected samples indoors (30 trials with three

[2]The noise from Ultrasonic 1 in Figure 10 is an extreme example, as there was faulty cabling. However, the altitude estimate tracks in spite of this noise.

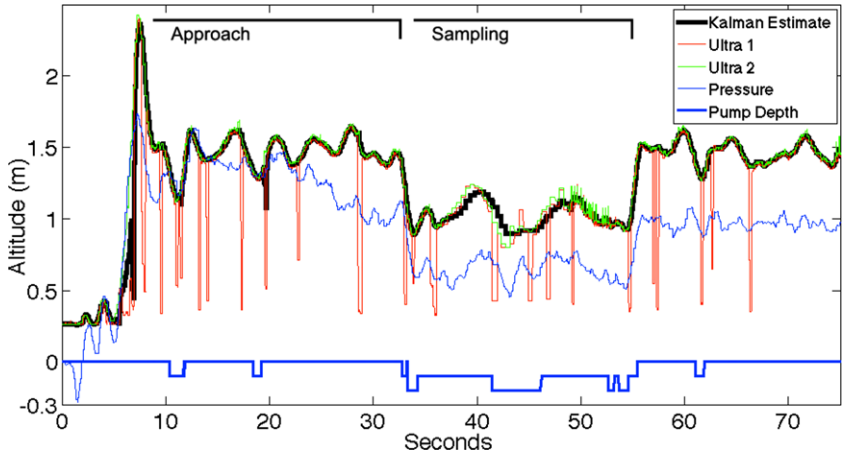

Figure 10. Vehicle altitude and pump depth while sampling outdoors.

Table IV. Sampling success rate.

Altitude	Trials	Samples	Full	$> \frac{1}{2}$	$< \frac{1}{2}$	% Full
Indoor	30	90	81	6	3	90.0
Vicon	15	45	41	3	1	91.1
Ultrasonic	15	45	40	3	2	88.9
Outdoor	28	84	70	11	3	83.3
Grand Total	58	174	151	17	6	86.8

samples each), 81 were full (90% success). To better understand the relation between the success rate and the use of our ultrasound and pressure altitude controller, half of the samples were collected using the altitude reported by the Vicon motion capture system. The second and third rows of Table IV show that the success rate is nearly the same for both Vicon and ultrasonic altitude, which indicates that ultrasonic rangers are suitable for height estimation over water. Of the indoor sample failures, six of nine were over half full. Failures were caused by the pump landing outside the fish tank or the pump failing to self-prime.

We performed similar outdoor experiments to test the effectiveness of the sampling system when controlled autonomously over water. The test site is shown in Figure 11 where we have permission from the United States Federal Aviation Administration (FAA) to perform UAV test flights, in the form of a "Certificate of Waiver or Authorization" (COA, 2014-CSA-17-COA). We programmed the system to collect three samples. Since our outdoor test facility has a water feature that is long but only 3 m wide, the computer controlled the yaw and z while a human pilot controlled the system in x and y. The results of this test are shown in Table IV. We repeated the outdoor sample mission 28 times, for a total of 84 samples, during winds from 1.5 to 5.8 m/s. The success rate for fully filled vials was 83.3%, with 11 of the remaining 14 over half full. Failures to pump outside were caused by variations in altitude, the pump not priming, and occasionally the mechanism would run slowly because of silt. Overall, within the wind and environmental

Figure 11. Sampling in wind at our outdoor test facilities.

Table V. Sampling success rate by wind speed and target altitude.

	Success Rate (% Full)					
	Wind Speed (m/s)					
Target Altitude (m)	0 − 2.7	2.7 − 3.5	3.5 − 4.5	4.5 − 5.3	5.3+	Total
0.72	100	95	92	76	87	92
0.82	90	79	86	65	80	82
0.92	85	89	89	71	70	83
1.02	88	64	49	50	47	60
1.12	10	37	42	30	43	34
TOTAL	81	73	69	56	66	71

constraints, the system demonstrated the ability to maintain altitude and retrieve samples.

4.3. Environmental Factors

Wind is a key environmental factor in any aerial field deployment. The FireFly is specified to operate by the manufacturer in winds up to 10 m/s with a payload while in GPS mode, and in our experience it can maintain an approximate position in an open area in winds as high as 15 m/s. However, when close to the water, even winds less than 10 m/s disrupt the system's ability to sample water successfully in several ways: 1) wind changes the air pressure around the vehicle, causing the pressure altimeter to register large and rapid changes in altitude, 2) wind blows the dangling tube away at an angle ($+30^{\circ}$), reducing the effective tube length, 3) wind disrupts water flow at the needle, causing less water to enter the capture vial, and 4) stronger winds appear to change "ground effect" behavior near the water by displacing the column of pressurized air under the vehicle to a position downwind, as observed by ripples in the water. We know from experience that wind perturbs altitude control and can bring the vehicle alarmingly close to a swim. Yet our mission requires that we fly close to achieve a high sampling success rate. During sampling, we set a "target altitude" that the vehicle attempts to maintain while pumping water into the vial. We want to find a target altitude that balances the increased risk of total failure while close to the water, with the increased sampling performance closer to the water. Therefore, we designed an experiment to test the effectiveness of the sampler at various target altitudes across a range of wind speeds.

We programmed the UAV to fly over the small water feature at our outdoor test facility (Figure 11) and sample three times, ascending between samples to 4 m. During this experiment, and as we did before, the computer controlled altitude and yaw, while a human backup pilot controlled x and y because of the narrow profile of the water feature at our outdoor test facility (< 3 m, about the same width as the GPS error). We measured wind speed using a portable weather station affixed to a tripod situated 5–6 m from the sample location at 2 m above the ground. The wind station records speed and direction at 4 Hz directly into the system's trace file. We average the wind speed during each sample event, and we verified the readings compared to measurement from a hand anemometer. We tested five target altitudes from 0.72 to 1.12 m in 0.10 m increments. We chose heights in this range because at a target altitude of 0.72 m in stronger winds the vehicle can get very close to the water, and at 1.12 m the pump barely touches the water. During this experiment, we overrode the risk management mechanisms triggered by the conductivity sensors, ultrasonic sensors, and altitude so we could continue to sample even though the altitude over water transgressed the safe operating boundaries specified by the risk management system. During the experiment, we changed the target altitude after each trial so that as the wind changed during the day, we could collect data at each target altitude across a range of wind speeds. We conducted 75 trials of three samples each in three days for a total of 225 samples, and we binned the results by wind speed. We chose the bin sizes so that each bin would have at least four samples.

The results for the sampling success rate are shown in Table V. The highest success rates occur at the lowest target altitude (0.72 m), and the highest altitude was the least successful at all wind speeds. This is because the pump remains completely submerged in spite of altitude perturbations. Even in the strongest winds measured during this test, the sampling success rate remains $\geq 70\%$ successful with a target altitude at or below 0.92 m. Between target altitudes 0.92 and 1.02 m there is a significant reduction in sampling success, indicating that in the proximity of 0.92 m we may find the sweet spot that lowers risk but can still result in a large number of success samples. Surprisingly, at the highest target altitude 1.12 m, the success rate increases more with some winds than with nearly no wind. It appears

Table VI. Minimum altitude (avg) by wind speed and target altitude.

	Average Minimum Altitude (m)					
	Wind Speed (m/s)					
Target Altitude (m)	0 − 2.7	2.7 − 3.5	3.5 − 4.5	4.5 − 5.3	5.3+	Total
0.72	0.48	0.49	0.43	0.43	0.35	0.43
0.82	0.56	0.60	0.52	0.45	0.43	0.51
0.92	0.69	0.71	0.54	0.61	0.51	0.61
1.02	0.75	0.76	0.77	0.55	0.65	0.70
1.12	0.88	0.88	0.86	0.78	0.77	0.83
TOTAL	0.67	0.69	0.62	0.56	0.54	

Table VII. Minimum altitude (avg) by wind speed and target altitude.

	Average Max Conductivity Reading (0-5, 5 is deepest)					
	Wind Speed (m/s)					
Target Altitude (m)	0 − 2.7	2.7 − 3.5	3.5 − 4.5	4.5 − 5.3	5.3+	Average
0.72	3.83	4.12	4.50	4.60	4.75	4.36
0.82	3.50	3.60	3.88	4.29	4.00	3.85
0.92	3.00	3.00	3.73	3.67	4.00	3.58
1.02	3.50	2.56	2.50	3.50	2.88	2.85
1.12	4.00	2.80	2.10	2.38	2.80	2.53
AVERAGE	3.57	3.21	3.26	3.60	3.73	

that as the wind speed increases, the increased variation in altitude allows the pump to be in the water long enough for the system to pump more water than at low wind speeds, when the pump is just barely submerged. Clearly, pumping longer will improve the success rate, and the main consequence of overfilling is wasted time and energy. These experiments help us find a baseline performance expectation from which we can seek a balance between time, energy, and success rate.

Although setting a lower target altitude increases the success rate, there is a lower limit. Table VI shows the minimum altitude over water during the sampling mission, averaged by bin. As wind speed increases, we tend to get closer to the water at some point during sampling. At 0.72 m target altitude in the strongest winds, we get within 0.35 cm of the water on average. This is probably too close even if the vehicle did not get wet, since we might get too close for the human backup pilot to recover the vehicle in case of an emergency.

Another way to measure how the proximity to the water changes with wind speed is to look at the water conductivity sensors. Table VII shows the maximal water conductivity sensor to touch the water during sampling, where a 1 means the first conductivity sensor located at the pump, 2 means the conductivity sensor 10 cm up the sampling tube from the pump, and 5 is the maximum depth.[3] In general, the vehicle gets closer to the water as wind speed increases.

We also investigated the potential impact of battery level on vehicle altitude. The normal battery levels range from 12.5 to 10.5 V, below which the Firefly alerts the user with an audible siren. During these experiments, we always changed the battery before the siren engaged, using each battery in four or five trials. Within this normal range of battery operation, we did not detect a significant correlation between the battery level and the minimal altitude or conductivity.

4.4. Sampling Technique: Hand vs. UAV Mechanism

We conducted an experiment to check whether water samples collected by the UAV mechanism exhibit similar water chemical properties as samples obtained through traditional hand-sampling methods. Potential differences include those caused by pumping, transit through the tube, agitation during flight, and changes in water properties during the delay between sample acquisition and sample

[3]Note that at the lowest wind speed, the conductivity sensors failed to read correctly due to a wiring problem during a series of samples, which resulted in higher than normal values.

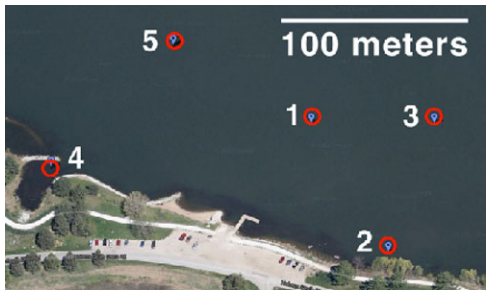

Figure 12. Holmes Lake sample locations.

measurement on land. The UAV was not flown, but rather held by a human operator in a kayak to ensure that both the hand and UAV samples were taken at the same time and place.

To verify the consistency between manual and UAV-based sampling, we sampled at five locations on Holmes Lake, Lincoln, NE. We collected two samples near shore and three closer to the middle of the lake, as shown in Figure 12. At each location, we took three samples by hand and three with the UAV mechanism for a total of 15 samples by each method. Overall it took approximately 2 h to collect these data due to the time to kayak, collect manual and UAV-mechanism samples, and to perform some onsite analysis and filtering. We estimate that collecting the samples with the UAV flying would take 20 min.

At each location we measured temperature, dissolved oxygen (DO),[4] sulfate, and chloride. By sampling both a dissolved gas and representative ions, we can assess the suitability of the UAV mechanism for scientific water sampling. Temperature and DO are measured at the sample location for the manual measurements and at shore once the UAV returns, since these properties change rapidly. Chloride and sulfate ions are measured in the lab using equipment[5] that is not easily portable, and these properties do not change rapidly after sampling and filtering. We measured DO as it is a key indicator of biological activity and because we suspected the UAV mechanism might bias the measurement through degassing during pumping or continued photosynthesis during transit. Sulfate and chloride ions occur naturally in most water, and their ratio in freshwater can indicate proximity to a saltwater source. But inland, chloride comes from many sources, including lawn fertilizers and road salt. High concentrations of chloride in organisms can induce osmotic stress, reduced fitness, or mortality.

We are primarily interested in verifying that the UAV mechanism does not induce a bias in the measurements. Figure 13(a) shows the DO as measured by hand at the location and with the UAV mechanism. The values at the five sample locations are close and show the same general trend in all five locations, implying that the UAV mechanism and delay (longer by kayak than by flying) has little impact on the DO. Also visible in this figure is the general upward trend between the sample locations. This was probably caused by increased photosynthesis over the 2 h of data collection, although sample location may also play a role in this variation. For instance, location 4 is probably higher than the general trend because it is closer to an enclosed bay and therefore likely to have more plants near the surface. Obtaining samples quickly by UAV could help to disambiguate these factors.

Sulfate and chloride concentrations shown in Figures 13(b) and 13(c) revealed some differences between hand methods and the UAV mechanism. These differences, however, can likely be attributed to typical sampling variation, and neither indicates a strong bias induced by the UAV mechanism. Further, the typical range for sulfate in lakes is between 10 and 60 mg/L (Orem, 2004), and for chloride it varies seasonally but usually is between 10 and 100 mg/L (Dodds, 2002), so the observed variation is minimal. We plan to perform additional field and lab tests to verify that these measurements are unbiased.

In contrast to the other measurements, Figure 13(d) shows that the temperature measured by hand at the sample location is nearly constant, while the temperature measured in samples from the UAV mechanism changed during transit, especially at locations 2 and 3. Future versions of system should measure water temperature at the sample location by mounting a temperature probe at the end of the pumping tube.

These experiments show that the UAV mechanism can collect samples that resemble those collected by hand. The UAV system, however, greatly reduces the effort and time needed to collect samples. This permits water scientists to obtain more samples within a single lake or river to develop a high-resolution map, for instance after a rainstorm to identify the source of the influx of chemical or biological contaminates. In addition, reducing the collection time is critical since many water properties, such as DO, fluctuate within hours, and using our UAV system would reduce collection time by nearly an order of magnitude.

5. LESSONS LEARNED

In this work, we have successfully developed an aerial water sampler that can obtain water samples from locations even in moderate winds. During development, we experienced numerous instructive failures. In this section, we discuss these lessons and what we learned from them.

Our first prototype explored vials suspended from a cord, but early flight tests showed that adding 60 g of water plus the mass of the vials induced unpredictable and hazardous flight dynamics because of pendulum effects.

[4]For DO and temperature, a single reading was obtained with the hand sensor at the location, but for the UAV mechanism it was tested on each of the three samples.

[5]Lab measurements use a Dionex Ion Chromatograph AS14A, made by ThermoFisher.

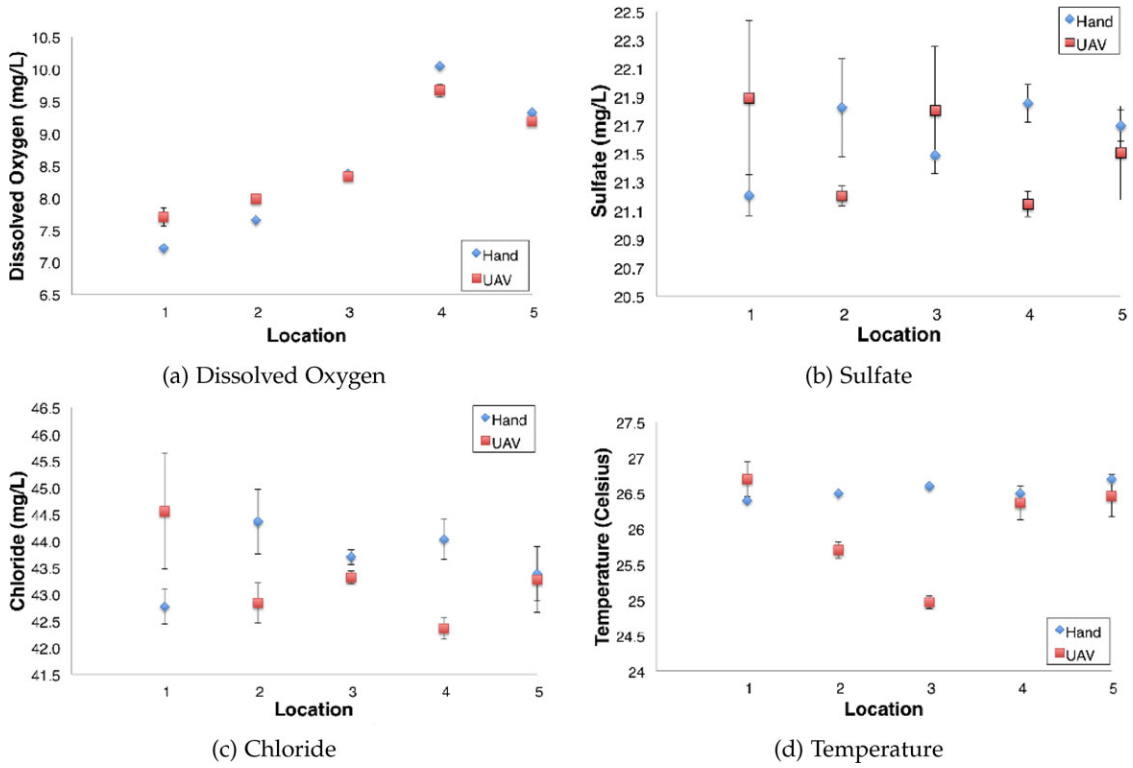

Figure 13. Water chemistry measurements from hand sampling and the UAV mechanism. Points represent the average of three replicate measurements, and error bars indicate ±1 standard error of the mean.

We considered a mechanism to "reel-in" samples, but we found it too complicated to have retractable sensor and communication cabling, or waterproof short-range wireless communication. We looked at drawing water up through the tube using suction, but found that only massive pumps (for a UAV) could draw water up 1 m. These options might be worth exploring with heavier-lift UAVs.

We also explored water hardening the UAV, sample chambers, and sampling mechanism, but our previous work in underwater sensor nodes convinced us that making any part waterproof adds unacceptable mass and undermines the speed and ease of swapping vials and batteries. In spite of not being waterproof, we have had only one completely debilitating interaction with water as well as some near misses where the landing gear and sampling mechanism touched the water but not the electronics. Fortunately, even after being fully submerged in freshwater, the AscTec Firefly survived after careful drying.

It surprised us somewhat that the lowest sampling target altitude 0.72 m was the most effective, because we had previously seen that the variability in the altitude during wind gusts would bring the system close enough to water to experience a "ground effect," causing rebound and oscillations in altitude that would degrade performance. However, we observed that in stronger winds, the UAV's downdraft is blown downwind, as we could see by the water ripples displaced almost the width of the UAV, and therefore the ground effect seemed negligible.

The risk management mechanisms react faster than our human backup pilots, and err on the side of caution. We found this worked well in most field trials, although at times pumping could have easily continued safely. This is actually similar to how novice human safety pilots act. In our experience, pilots frequently take over too soon until they grow more comfortable with the system limits. Likewise, over time we tuned the risk management system to accept a wider range of behavior in the field.

6. CONCLUSIONS AND FUTURE WORK

Water sampling has become a key activity in effectively managing our freshwater resources and maintaining public health. Developing approaches and systems for efficient and effective water monitoring will increase in importance over the coming decades. In this paper, we have demonstrated a novel mechanism for sampling water autonomously from a UAV that requires significantly less effort than existing techniques and is nearly an order of magnitude faster. The system can safely fly close to water and collect three 20 ml samples per flight. We verified that the water properties of the

samples collected by the UAV match those collected through traditional manual sampling techniques. This shows that this system can be used by water scientists to improve the spatial scale and temporal resolution of water sampling. We introduced our risk management framework used to assess and respond to hazardous circumstances. Lastly, we conducted 75 outdoor trials of three samples over a range of wind speeds up to 5.8 m/s.

Our future efforts include further operation and evolution of the system outdoors, especially how this platform might be used with adaptive sampling, sampling at greater depths, and in combination with other sensing and sampling mechanisms deployed in bodies of water. We plan to characterize our risk management framework as part of a longer-term analysis of failure modes and system reliability. We are pursuing methods for measuring the quantity of water in the vials. We intend to explore how the system performs on a more diverse set of bodies of water, including those with continuous flows and waves. We are working on implementing an onboard wind vector estimate following the methods from recent work (Neumann, Asadi, Lilienthal, Bartholmai, & Schiller, 2012) which utilizes onboard sensors. This will enable the system to estimate the wind and adjust the target altitude accordingly. We are also in the process of implementing and evaluating the usability of a user interface for the limnologists and nonexpert operators that balances manual control with autonomous behavior with the goal of maintaining system and operator safety. We plan to examine the duration of the "flushing" phase with our collaborators to ensure clean samples. Further, we would like to push some water analysis onto the platform to avoid collecting samples that do not meet required criteria. In addition, we will explore a line of inquiry pertaining to operational safety, as these systems are intended to be reliable tools in the hands of field scientists.

ACKNOWLEDGMENTS

We would like to thank our limnologist and environmental engineering partners at UC Berkeley, Dr. Michael Hamilton and Dr. Sally Thompson, for their continuous support of these efforts. Deep thanks to mechanical engineer Baoliang Zhao for his clever chassis design. This work was also greatly assisted by Hengle Jiang, Dave Anthony, Adam Taylor, Jacob Greenwood, Christa Webber, Emily Waring, Seth McNeil, Jared Ostdiek, Najeeb W. Najeeb, Daniel Rogge, and the NIMBUS Lab. This work was partially supported by USDA #2013-67021-20947, AFOSR #FA9550-10-1-0406, NSF IIS-1116221, NSF CSR-1217400, NDEQ grant #56-1131, and a development grant from ORED-UNL. Any opinions, findings, and conclusions or recommendations expressed in this material are those of the authors and do not necessarily reflect the views of these agencies.

REFERENCES

Achtelik, M. C., Doth, K.-M., Gurdan, D., & Stumpf, J. (2012). Design of a multi rotor MAV with regard to efficiency, dynamics and redundancy. In AIAA Guidance, Navigation, and Control Conference (pp. 1–17).

Aquacopters (2012). Aquacopters. http://www.aquacopters.com/. [online, accessed 15-June-2014].

Bachrach, A., He, R., & Roy, N. (2009). Autonomous flight in unknown indoor environments. International Journal of Micro Air Vehicles, 1(4), 217–228.

Bills, C., Chen, J., & Saxena, A. (2011). Autonomous mav flight in indoor environments using single image perspective cues. In 2011 IEEE International Conference on Robotics and Automation (ICRA) (pp. 5776–5783). IEEE.

Bird, L. E., Sherman, A., & Ryany, J. (2007). Development of an active, large volume, discrete seawater sampler for autonomous underwater vehicles. In OCEANS (pp. 1–5). IEEE.

Clothier, R. A., & Walker, R. A. (2012). The safety risk management of unmanned aircraft systems. Handbook of Unmanned Aerial Vehicles Springer Netherlands 2014, pp. 2229–2275.

Cruz, N. A., & Matos, A. C. (2008). The MARES AUV, a modular autonomous robot for environment sampling. In OCEANS (pp. 1–6). IEEE.

Dezfuli, H., Benjamin, A., Everett, C., Maggio, G., Stamatelatos, M., Youngblood, R., Guarro, S., et al. (2011). Nasa risk management handbook. Technical report, NASA.

Dodds, W. K. (2002). Freshwater ecology: Concepts and environmental applications. San Diego: Academic Press.

Dodds, W. K., Bouska, W. W., Eitzmann, J. L., Pilger, T. J., Pitts, K. L., Riley, A. J., Schloesser, J. T., & Thornbrugh, D. J. (2009). Eutrophication of U.S. freshwaters: Analysis of potential economic damages. Environmental Science & Technology, 43(1), 12–19.

Dorofee, A. J., Walker, J. A., Alberts, C. J., Higuera, R. P., & Murphy, R. L. (1996). Continuous risk management guidebook. Technical report, DTIC Document.

Dunbabin, M., & Grinham, A. (2010). Experimental evaluation of an autonomous surface vehicle for water quality and greenhouse gas emission monitoring. In 2010 IEEE International Conference on Robotics and Automation (ICRA) (pp. 5268–5274). IEEE.

Dunbabin, M., Grinham, A., & Udy, J. (2009). An autonomous surface vehicle for water quality monitoring. In Proceedings of the Australasian Conference on Robotics and Automation (ACRA) (vol. 13).

Eaton, A. D., & Franson, M. A. H. (2005). Standard methods for the examination of water & wastewater. American Public Health Association.

Erickson, A. J., Weiss, P. T., & Gulliver, J. S. (2013). Water sampling methods. In Optimizing Stormwater Treatment Practices (pp. 163–192). New York: Springer.

Faust, A., Palunko, I., Cruz, P., Fierro, R., & Tapia, L. (2013). Learning swing-free trajectories for uavs with a suspended load. In 2013 IEEE International Conference

on Robotics and Automation (ICRA) (pp. 4902–4909). IEEE.

Göktoğan, A. H., Sukkarieh, S., Bryson, M., Randle, J., Lupton, T., & Hung, C. (2010). A rotary-wing unmanned air vehicle for aquatic weed surveillance and management. Journal of Intelligent and Robotic Systems, 57, 467–484.

Harel, D. (1987). Statecharts: A visual formalism for complex systems. Science of Computer Programming, 8(3), 231–274.

ITOPF, I. (2012). Sampling and monitoring of marine oil spills. http://www.itopf.com/information-services/publications/documents/TIP14SamplingandMonitoringofMarineOilSpills.pdf [online; accessed 1-July-2014].

Jain, S., Nuske, S., Chambers, A., Yoder, L., Cover, H., Chamberlain, L., Scherer, S., & Singh, S. (2013). Autonomous river exploration. In Proceedings of The 9th International Conference on Field and Service Robots (FSR). Brisbane, Australia (vol. 5).

Jiang, H., Elbaum, S., & Detweiler, C. (2013). Reducing failure rates of robotic systems though inferred invariants monitoring. In 2013 IEEE/RSJ International Conference on Intelligent Robots and Systems (IROS) (pp. 1899–1906). IEEE.

Jimenez-Cano, A., Martin, J., Heredia, G., Ollero, A., & Cano, R. (2013). Control of an aerial robot with multi-link arm for assembly tasks. In 2013 IEEE International Conference on Robotics and Automation (ICRA) (pp. 4916–4921). IEEE.

Kendoul, F. (2012). Survey of advances in guidance, navigation, and control of unmanned rotorcraft systems. Journal of Field Robotics, 29(2), 315–378.

Kulić, D., & Croft, E. A. (2005). Safe planning for human-robot interaction. Journal of Robotic Systems, 22(7), 383–396.

Lacevic, B., & Rocco, P. (2010). Kinetostatic danger field—A novel safety assessment for human-robot interaction. In 2010 IEEE/RSJ International Conference on Intelligent Robots and Systems (IROS) (pp. 2169–2174). IEEE.

Maxbotix (2014). MaxBotix Ultrasonic Sensors. http://www.maxbotix.com [online; accessed 15-June-2014].

Melo, J., & Matos, A. (2012). Bottom estimation and following with the MARES AUV. In Oceans (pp. 1–8). IEEE.

Merz, T., & Kendoul, F. (2013). Dependable low-altitude obstacle avoidance for robotic helicopters operating in rural areas. Journal of Field Robotics, 30(3), 439–471.

Merz, T., Rudol, P., & Wzorek, M. (2006). Control system framework for autonomous robots based on extended state machines. In 2006 International Conference on Autonomic and Autonomous Systems (p. 14). IEEE.

Michael, N., Fink, J., & Kumar, V. (2011). Cooperative manipulation and transportation with aerial robots. Autonomous Robots, 30(1), 73–86.

Montemerlo, M., Pineau, J., Roy, N., Thrun, S., & Verma, V. (2002). Experiences with a mobile robotic guide for the elderly. In AAAI/IAAI (pp. 587–592).

Neumann, P. P., Asadi, S., Lilienthal, A. J., Bartholmai, M., & Schiller, J. H. (2012). Autonomous gas-sensitive microdrone: Wind vector estimation and gas distribution mapping. IEEE Robotics & Automation Magazine, 19(1), 50–61.

Ore, J. P., Elbaum, S., Burgin, A., Zhao, B., & Detweiler, C. (2013). Autonomous aerial water sampling. In Proceedings of The 9th International Conference on Field and Service Robots (FSR). Brisbane, Australia (vol. 5, pp. 137–151).

Orem, W. H. (2004). Impacts of sulfate contamination on the Florida Everglades ecosystem. Fact Sheet FS 109–03. Reston, Virginia, U.S. Geological Survey.

Orsag, M., Korpela, C., Bogdan, S., & Oh, P. (2014). Valve turning using a dual-arm aerial manipulator. In 2014 International Conference on Unmanned Aircraft Systems (ICUAS) (pp. 836–841). IEEE.

Pilliod, D. S., Goldberg, C. S., Laramie, M. B., & Waits, L. P. (2012). Application of Environmental DNA for Inventory and Monitoring of Aquatic Species. Fact Sheet FS 2012-3146 Corvallis, Oregon, U.S. Geological Survey.

QuadH2O (2014). Water resistant multirotor. http://www.quadh2o.com/ [online; accessed 30-June-2014].

Rahimi, M., Pon, R., Kaiser, W., Sukhatme, G., Estrin, D., & Srivastava, M. (2004). Adaptive sampling for environmental robotics. In Proceedings of the IEEE International Conference on Robotics and Automation (vol. 4, pp. 3537–3544).

Ritz, R., & D'Andrea, R. (2013). Carrying a flexible payload with multiple flying vehicles. In 2013 IEEE/RSJ International Conference on Intelligent Robots and Systems (IROS) (pp. 3465–3471). IEEE.

Ross, S., Melik-Barkhudarov, N., Shankar, K. S., Wendel, A., Dey, D., Bagnell, J. A., & Hebert, M. (2013). Learning monocular reactive uav control in cluttered natural environments. In 2013 IEEE International Conference on Robotics and Automation (ICRA) (pp. 1765–1772). IEEE.

Sattar, J., & Dudek, G. (2014). Reducing uncertainty in human-robot interaction, a cost analysis approach. In Experimental Robotics (pp. 81–95). Springer.

Scherer, S., Rehder, J., Achar, S., Cover, H., Chambers, A., Nuske, S., and Singh, S. (2012). River mapping from a flying robot: State estimation, river detection, and obstacle mapping. Autonomous Robots, 33(1-2), 189–214.

Scherer, S., Singh, S., Chamberlain, L., & Saripalli, S. (2007). Flying fast and low among obstacles. In 2007 IEEE International Conference on Robotics and Automation (pp. 2023–2029). IEEE.

Schmid, K., Lutz, P., Tomić, T., Mair, E., & Hirschmüller, H. (2014). Autonomous vision-based micro air vehicle for indoor and outdoor navigation. Journal of Field Robotics, 31(4), 537–570.

Schwarzbach, M., Laiacker, M., Mulero-Pázmány, M., & Kondak, K. (2014). Remote water sampling using flying robots. In 2014 International Conference on Unmanned Aircraft Systems (ICUAS) . IEEE.

Shen, S., Michael, N., & Kumar, V. (2011). Autonomous multi-floor indoor navigation with a computationally constrained mav. In 2011 IEEE International Conference on Robotics and Automation (ICRA) (pp. 20–25). IEEE.

Sreenath, K., Michael, N., & Kumar, V. (2013). Trajectory generation and control of a quadrotor with a cable-suspended

load a differentially-flat hybrid system. In Proceedings of the IEEE International Conference on Robotics and Automation (pp. 4888–4895).

TCSMicropumps (2014). TCS Micropumps, UK. Model M200S-SUB. http://micropumps.co.uk/TCSM200range.htm [online; accessed 15-June-2014].

The United Nations Children's Fund (UNICEF)/World Health Organization (WHO), Johansson, E., & Wardlaw, T. (2009). Diarrhoea: Why children are still dying and what can be done. In WHO Library Cataloging-in-Publication Data.

Thomas, J., Polin, J., Sreenath, K., & Kumar, V. (2013). Avian-inspired grasping for quadrotor micro uavs. In ASME 2013 International Design Engineering Technical Conferences and Computers and Information in Engineering Conference (pp. V06AT07A014–V06AT07A014). American Society of Mechanical Engineers.

WHO, W. H. O. (2004). Guidelines for drinking-water quality: Recommendations (vol. 1). World Health Organization.

Wilde, F. D., Radtke, D. B., Gibs, J., & Iwatsubo, R. T. (1998). National field manual for the collection of water-quality data: Field measurements. U.S. Department of the Interior, U.S. Geological Survey.

Wurm, K. M., Hornung, A., Bennewitz, M., Stachniss, C., & Burgard, W. (2010). Octomap: A probabilistic, flexible, and compact 3d map representation for robotic systems. In Proceedings of the ICRA 2010 Workshop on Best Practice in 3D Perception and Modeling for Mobile Manipulation (vol. 2).

Zhang, B., & Sukhatme, G. (2007). Adaptive sampling for estimating a scalar field using a robotic boat and a sensor network. In 2007 IEEE International Conference on Robotics and Automation (pp. 3673–3680). IEEE.